Reprinted with permission from the publisher.
Electrical Engineering (Archiv fur Elektrotechnik).
ISSN: 0948-7921 (Print), 1432-0487 (Online)
DOI: 10.1007/s00202-006-0327-5
The original publication is available at www.springerlink.com
http://www.springerlink.com/openurl.asp?genre=article&id=doi:10.1007/s00202-006-0327-5
© 2006 by authors and © 2006 Springer Science+Business Media

APPENDIX II

Publication P2

Burakov, A., Arkkio, A. 2006. Low-order parametric force model for a salient-pole synchronous machine with eccentric rotor. *Electrical Engineering (Archiv fur Elektrotechnik)*, Springer Berlin / Heidelberg, Vol. 89, No. 2, pp. 127-136.

Low-order parametric force model for a salient-pole synchronous machine with eccentric rotor

ANDREJ BURAKOV AND ANTERO ARKKIO

Helsinki University of Technology, Laboratory of Electromechanics

P.O. Box 3000, FIN-02015 HUT, Finland

tel. +358 9 451 2381

fax +358 9 451 2991

email: Andrej.Burakov@tkk.fi

Abstract

In this paper, a low-order parametric force model to represent the electromagnetic force on an eccentric rotor of a salient-pole synchronous machine was developed and verified. The force model with parameters estimated from the results of impulse method showed excellent performance. The proposed model allowed quick and accurate calculation of the electromagnetic force at the desired whirling frequency values and provided an opportunity to effectively combine the electromagnetic and mechanical analyses of electrical machine. Besides, results presented in this paper also verified the suitability of computationally efficient impulse method for the analysis of a synchronous machine.

Keywords: *salient-pole synchronous machine, rotor eccentricity, parametric force model, impulse method*

Abbreviations

MMF, magnetomotive force
FEA, finite element analysis
FRF, frequency response function;

1 Introduction

Electrical machine belongs to a category of electro-magneto-mechanical devices. Thus, when designing an electrical machine and/or optimising its

performance it has to be analysed from mechanical, electromagnetic and also thermal points of view. And, preferably, these analyses must be coupled.

To achieve accurate results an electrical machine is often studied employing the Finite Element Analysis (FEA) but the calculations are rather time-consuming. Coupling several analyses would increase the computational time even further. Therefore, it would be a great advantage to study the behaviour of an electrical machine using simpler and, hence, faster approaches. A simple parametric model representing the electromagnetic force acting between the eccentric rotor and stator of an electrical machine can be a good example. This model supplied as an input to the mechanical analysis of the machine can greatly reduce the computational task and enable the solution of a coupled electro-magneto-mechanical problem to be obtained with reasonable time-consumption.

Rotor eccentricity occurs when the rotor axis does not coincide with the stator bore axis but instead whirls around the latter at a certain radius and angular speed (called whirling radius and whirling angular speed). The occurrence of eccentric rotor in an electrical machine is not a rare occasion: due to manufacturing tolerances, wear of bearings, imperfect rotor mounting on its bearings and other reasons some degree of rotor eccentricity is always present. Depending on the angular speed and radius of the whirling motion the electromagnetic force due to it can be significant. This force, acting roughly in the direction of the shortest air gap length, tries to further increase the eccentricity magnitude and may cause a serious damage to the machine or even the whole drive.

Importance of the problems associated with the eccentric rotor in electrical machine has already been recognised more than one hundred years ago [1]. Many papers have been published on this subject. They mainly focus on two special cases of the whirling motion i.e. the static eccentricity, which occurs when the rotor axis is displaced from the stator bore axis but remains stationary with respect to it; and dynamic eccentricity, taking place when the whirling angular speed is equal to the mechanical angular speed of the rotor motion. The absolute majority of the papers published deal with an induction machine [2], [3], [4], [5], [6] and substantially fewer carry out the study on a salient-pole synchronous machine [7], [8], [9]. Similarly to an induction machine, the rotor of a synchronous machine can be equipped with the damper winding (called also, rotor cage), which is known to effectively attenuate the force associated with rotor eccentricity [10], [11]. But the rotor saliency and parallel connections in the stator winding render the analysis of a synchronous machine considerably more complicated.

Besides the static and dynamic eccentricities, the rotor whirling may also occur at other angular speeds. Früchtenicht et al. [12] have presented an analytical method to investigate the electromagnetic forces caused by eccentric rotor in an induction machine. The method was based on the permeance harmonic analysis and could be used to study whirling motion at various angular speeds.

Using Früchtenicht's achievements, Arkkio et al. [13] developed a low-order parametric model to represent the electromagnetic force acting on eccentric rotor of an induction machine in a wide whirling frequency range. Tenhunen et al. [14] have successfully applied an impulse method to determine the parameters of the force model presented by Arkkio et al.

In this paper, we develop and verify a low-order parametric force model for a salient-pole synchronous machine with eccentric rotor. Only the circular rotor whirling in steady state is considered. The machine is equipped with the rotor cage and the stator winding is assumed to have no parallel paths. The model accounts for the saturation of iron core, effects of slotting and equalising currents in the rotor cage. Force model parameters are calculated from the results provided by the computationally efficient impulse method applied in the FEA. The force model with estimated parameters shows an excellent performance in a wide whirling frequency range. The proposed force model has several major advantages:

1) It allows simple, quick and accurate calculation of the electromagnetic force at a desired whirling frequency value or in a certain range of whirling frequencies
2) The same model parameters can be directly applied to calculate the electromagnetic force at different whirling radius and whirling angular speed values
3) The model offers an attractive opportunity to be integrated into the mechanical analysis to study the electromechanical interaction in electrical machines.

There also are limitations of this force model:

1) Every time the operating point (supply voltage, load torque, etc.) of a machine is changed a new set of force model parameters has to be established
2) This force model cannot be applied for a synchronous machine with parallel paths in the stator winding.

Additionally, results presented in this paper verified the suitability of the computationally efficient impulse method for the analysis of a synchronous machine.

The paper is organised as follows: the introductory part is followed by *Methods of analysis* where the force model expression is developed starting from the basic two-axis equations for a synchronous machine. The performance of the force model is shown in *Results* part. The main achievements and a concise summary of the work accomplished are presented, respectively, in *Discussions* and *Conclusions*, at the end of the paper.

2 Methods of analysis

2.1 Two-axis model of a salient-pole synchronous machine

In this work, only the steady state operation mode of a synchronous machine is studied. Due to the rotor saliency the air gap length between the rotor and stator is not constant along the circumference of a machine: it is much smaller on the axis of a rotor pole (direct or d-axis) than between the neighbouring poles (quadrature or q-axis). Therefore, a synchronous machine is studied in rotor reference frame where the air gap permeance values for d- and q-axis are constant, independent of rotor position (if no eccentricity is present). The origin of the rotor reference frame is fixed to the stator bore axis and rotates at an angular speed of the rotor. The stator and rotor are assumed to be perpendicular to the d-q plane and the magnetic field in the core region is assumed to be two-dimensional and parallel to this plane. Although, the field winding magnetomotive force (MMF) in a salient-pole synchronous machine is constant within the angular length of a rotor pole, hereafter, we will use the sinusoidal distribution of this MMF. This will simplify the magnetic field analysis and have almost no effect on the spatial distribution of the magnetic flux density in the air gap. More details on this simplification are given in section 2.2.

Using the aforementioned assumptions the voltage equations for a salient-pole synchronous machine in rotor frame of reference are

$$\begin{aligned}
U_{\mathrm{d}}^{\mathrm{r}} &= R_{\mathrm{a}} i_{\mathrm{d}}^{\mathrm{r}} + \frac{\partial \Psi_{\mathrm{d}}^{\mathrm{r}}}{\partial t} - p\omega_{\mathrm{m}} \Psi_{\mathrm{q}}^{\mathrm{r}} \\
U_{\mathrm{q}}^{\mathrm{r}} &= R_{\mathrm{a}} i_{\mathrm{q}}^{\mathrm{r}} + \frac{\partial \Psi_{\mathrm{q}}^{\mathrm{r}}}{\partial t} + p\omega_{\mathrm{m}} \Psi_{\mathrm{d}}^{\mathrm{r}} \\
U_{\mathrm{f}}^{\mathrm{r}} &= R_{\mathrm{f}} i_{\mathrm{f}}^{\mathrm{r}} + \frac{\partial \Psi_{\mathrm{f}}^{\mathrm{r}}}{\partial t} \qquad , \quad (1) \\
U_{\mathrm{D}}^{\mathrm{r}} &= R_{\mathrm{D}} i_{\mathrm{D}}^{\mathrm{r}} + \frac{\partial \Psi_{\mathrm{D}}^{\mathrm{r}}}{\partial t} = 0 \\
U_{\mathrm{Q}}^{\mathrm{r}} &= R_{\mathrm{Q}} i_{\mathrm{Q}}^{\mathrm{r}} + \frac{\partial \Psi_{\mathrm{Q}}^{\mathrm{r}}}{\partial t} = 0
\end{aligned}$$

here, subscripts d, q refer to the stator windings on d- and q-axis respectively, D and Q refer to the damper winding quantities. Subscript f corresponds to the field winding quantities. Superscript r refers to the rotor frame of reference. R_{a} is the armature resistance, p is the number of pole-pairs of a machine, ω_{m} is the mechanical angular speed of the rotor motion.

Equations for magnetic flux linkages are

$$
\begin{aligned}
\Psi_{\mathrm{d}}^{\mathrm{r}} &= L_{\mathrm{d}} i_{\mathrm{d}}^{\mathrm{r}} + L_{\mathrm{md}} \left(i_{\mathrm{f}}^{\mathrm{r}} + i_{\mathrm{D}}^{\mathrm{r}} \right) \\
\Psi_{\mathrm{q}}^{\mathrm{r}} &= L_{\mathrm{q}} i_{\mathrm{q}}^{\mathrm{r}} + L_{\mathrm{mq}} i_{\mathrm{Q}}^{\mathrm{r}} \\
\Psi_{\mathrm{f}}^{\mathrm{r}} &= L_{\mathrm{f}} i_{\mathrm{f}}^{\mathrm{r}} + L_{\mathrm{md}} \left(i_{\mathrm{d}}^{\mathrm{r}} + i_{\mathrm{D}}^{\mathrm{r}} \right) + L_{\mathrm{fD}} i_{\mathrm{D}}^{\mathrm{r}} \\
\Psi_{\mathrm{D}}^{\mathrm{r}} &= L_{\mathrm{D}} i_{\mathrm{D}}^{\mathrm{r}} + L_{\mathrm{md}} \left(i_{\mathrm{f}}^{\mathrm{r}} + i_{\mathrm{d}}^{\mathrm{r}} \right) + L_{\mathrm{fD}} i_{\mathrm{f}}^{\mathrm{r}} \\
\Psi_{\mathrm{Q}}^{\mathrm{r}} &= L_{\mathrm{Q}} i_{\mathrm{Q}}^{\mathrm{r}} + L_{\mathrm{mq}} i_{\mathrm{q}}^{\mathrm{r}}
\end{aligned}
\quad . \qquad (2)
$$

The terms $L_{\mathrm{fD}} i_{\mathrm{D}}^{\mathrm{r}}$ and $L_{\mathrm{fD}} i_{\mathrm{f}}^{\mathrm{r}}$ show that there exists a magnetic coupling between the damper and field windings caused by the mutual flux component, which is not linked with the stator winding. In the following, these terms are neglected.

We define the equivalent number of turns in series of the stator winding as $N_{\mathrm{se}} = 4 k_{\mathrm{sw}} N_{\mathrm{s}} / \pi$, where N_{s} is the number of turns in series and k_{sw} is the winding factor of the stator winding.

The damper winding in the rotor can be transformed into two equivalent windings located on d- and q- axis separately. Moreover, the equivalent damper windings currents can be referred to as having the same number of equivalent turns in series as the stator current

$$
\begin{aligned}
i_{\mathrm{De}}^{\mathrm{r}} &= \frac{2 Q_{\mathrm{r,D}}}{3 \pi N_{\mathrm{se}}} i_{\mathrm{D}}^{\mathrm{r}} \\
i_{\mathrm{Qe}}^{\mathrm{r}} &= \frac{2 Q_{\mathrm{r,Q}}}{3 \pi N_{\mathrm{se}}} i_{\mathrm{Q}}^{\mathrm{r}}
\end{aligned}
\quad , \qquad (3)
$$

here, $Q_{\mathrm{r,D}}$ and $Q_{\mathrm{r,Q}}$ are the numbers of rotor cage bars on d- and q- axis respectively.

Considering only the fundamental components the system of equations (1) is rewritten as

$$
\begin{aligned}
U_{\mathrm{d},p}^{\mathrm{r}} &= R_{\mathrm{a},p} i_{\mathrm{d},p}^{\mathrm{r}} + \frac{\partial \Psi_{\mathrm{d},p}^{\mathrm{r}}}{\partial t} - p \omega_{\mathrm{m}} \Psi_{\mathrm{q},p}^{\mathrm{r}} \\
U_{\mathrm{q},p}^{\mathrm{r}} &= R_{\mathrm{a},p} i_{\mathrm{q},p}^{\mathrm{r}} + \frac{\partial \Psi_{\mathrm{q},p}^{\mathrm{r}}}{\partial t} + p \omega_{\mathrm{m}} \Psi_{\mathrm{d},p}^{\mathrm{r}} \\
U_{\mathrm{f},p}^{\mathrm{r}} &= R_{\mathrm{f},p} i_{\mathrm{f},p}^{\mathrm{r}} + \frac{\partial \Psi_{\mathrm{f},p}^{\mathrm{r}}}{\partial t} \\
U_{\mathrm{D},p}^{\mathrm{r}} &= R_{\mathrm{D},p} i_{\mathrm{De},p}^{\mathrm{r}} + \frac{\partial \Psi_{\mathrm{D},p}^{\mathrm{r}}}{\partial t} = 0 \\
U_{\mathrm{Q},p}^{\mathrm{r}} &= R_{\mathrm{Q},p} i_{\mathrm{Qe},p}^{\mathrm{r}} + \frac{\partial \Psi_{\mathrm{Q},p}^{\mathrm{r}}}{\partial t} = 0
\end{aligned}
\quad , \qquad (4)
$$

and the system of equations (2)

$$
\begin{aligned}
\Psi^{\mathrm{r}}_{\mathrm{d},p} &= L_{\mathrm{d},p} i^{\mathrm{r}}_{\mathrm{d},p} + L_{\mathrm{md},p}\left(i^{\mathrm{r}}_{\mathrm{f},p} + i^{\mathrm{r}}_{\mathrm{De},p}\right) \\
\Psi^{\mathrm{r}}_{\mathrm{q},p} &= L_{\mathrm{q},p} i^{\mathrm{r}}_{\mathrm{q},p} + L_{\mathrm{mq},p} i^{\mathrm{r}}_{\mathrm{Qe},p} \\
\Psi^{\mathrm{r}}_{\mathrm{f},p} &= L_{\mathrm{f},p} i^{\mathrm{r}}_{\mathrm{f},p} + L_{\mathrm{md},p}\left(i^{\mathrm{r}}_{\mathrm{d},p} + i^{\mathrm{r}}_{\mathrm{De},p}\right) \quad , \qquad (5) \\
\Psi^{\mathrm{r}}_{\mathrm{D},p} &= L_{\mathrm{D},p} i^{\mathrm{r}}_{\mathrm{De},p} + L_{\mathrm{md},p}\left(i^{\mathrm{r}}_{\mathrm{f},p} + i^{\mathrm{r}}_{\mathrm{d},p}\right) \\
\Psi^{\mathrm{r}}_{\mathrm{Q},p} &= L_{\mathrm{Q},p} i^{\mathrm{r}}_{\mathrm{Qe},p} + L_{\mathrm{mq},p} i^{\mathrm{r}}_{\mathrm{q},p}
\end{aligned}
$$

here, subscript p besides referring to the number of pole-pairs of the machine represents also the corresponding order of the space-harmonic.

The rotor cage consists of a number of short-circuited bars and, thus, numerous current harmonics are induced in it. Applying the discrete Fourier transform the cage ring currents can be represented as

$$
\begin{aligned}
i^{\mathrm{r}}_{\mathrm{D}} &= \sum_{m=1}^{N_{\max}} \mathrm{Re}\left(\underline{i}^{\mathrm{r}}_{\mathrm{D},m}\right) \\
i^{\mathrm{r}}_{\mathrm{Q}} &= \sum_{m=1}^{N_{\max}} \mathrm{Re}\left(\underline{i}^{\mathrm{r}}_{\mathrm{Q},m}\right)
\end{aligned}
\quad , \qquad (6)
$$

here, $N_{\max}$ is the highest order of rotor cage current harmonic. It has to be mentioned that not all of the current harmonics between the first and $N_{\max}$ are induced in the rotor cage. Some of them, with zero winding factors, will be missing. Due to the rotor cage asymmetry, winding factors of the individual circuits consisting of two neighbouring bars connected by the end-ring segments can differ from each other. This would allow for different current frequency spectra of the individual rotor cage circuits.

2.2 Magnetomotive forces (MMFs)

MMF on d-axis consists of MMFs created by the stator, damper and field winding currents

$$F^{\mathrm{r}}_{\mathrm{dt}} = F^{\mathrm{r}}_{\mathrm{d}} + F^{\mathrm{r}}_{\mathrm{D}} + F^{\mathrm{r}}_{\mathrm{f}} . \qquad (7)$$

q-axis MMF consists of contributions by the stator and damper windings only

$$F^{\mathrm{r}}_{\mathrm{qt}} = F^{\mathrm{r}}_{\mathrm{q}} + F^{\mathrm{r}}_{\mathrm{Q}} . \qquad (8)$$

We assume that the stator is equipped with a symmetrical three-phase winding and an integral number of slots per pole per phase. This type of winding produces the harmonic currents with ordinal numbers $\upsilon = p\left(1 \pm 6c\right)$, $c = 0, 1, 2, \ldots$ The fundamental component, $c = 0$, is the most important and the MMF produced by it

will be studied in this section. The spatial distribution of the MMF produced by the fundamental stator current component can be written as

$$\begin{aligned} F^{\mathrm{r}}_{\mathrm{d},p}(\varphi) &= \mathrm{Re}\left\{\left(\frac{3}{2}\frac{N_{\mathrm{se}}}{2p}i^{\mathrm{r}}_{\mathrm{d},p}\right)\cdot \mathrm{e}^{\mathrm{j}p\varphi}\right\} = \mathrm{Re}\left(F^{\mathrm{r}}_{\mathrm{d},p}\cdot \mathrm{e}^{\mathrm{j}p\varphi}\right) = \mathrm{Re}\left(\underline{F}^{\mathrm{r}}_{\mathrm{d},p}\right) \\ F^{\mathrm{r}}_{\mathrm{q},p}(\varphi) &= \mathrm{Re}\left\{\left(\frac{3}{2}\frac{N_{\mathrm{se}}}{2p}i^{\mathrm{r}}_{\mathrm{q},p}\right)\cdot \mathrm{e}^{\mathrm{j}p\varphi}\right\} = \mathrm{Re}\left(F^{\mathrm{r}}_{\mathrm{q},p}\cdot \mathrm{e}^{\mathrm{j}p\varphi}\right) = \mathrm{Re}\left(\underline{F}^{\mathrm{r}}_{\mathrm{q},p}\right) \end{aligned}, \qquad (9)$$

here, $F^{\mathrm{r}}_{\mathrm{d},p}$ is the fundamental MMF component in the direction of d-axis, and φ is the angular coordinate in the rotor reference frame.

As this study is primarily concerned with the steady state operation mode the presence of the fundamental MMF component produced by the damper winding is eliminated. This elimination is justified by the fact that in synchronous machine operating in a steady state mode the fundamental magnetic field component passing through the damper winding has a constant magnitude and is stationary with respect to the winding. Thus, there are no fundamental voltages induced in the damper winding, no fundamental currents and, hence, no fundamental MMF produced by this winding. Taking into account the other components of the rotor cage current (equation (6)) yields

$$\begin{aligned} F^{\mathrm{r}}_{\mathrm{D},m}(\varphi) &= \sum_{\substack{m=1\\ m\neq p}}^{N_{\max}} \mathrm{Re}\left(\underline{F}^{\mathrm{r}}_{\mathrm{D},m}\mathrm{e}^{\mathrm{j}m\varphi}\right) \\ F^{\mathrm{r}}_{\mathrm{Q},m}(\varphi) &= \sum_{\substack{m=1\\ m\neq p}}^{N_{\max}} \mathrm{Re}\left(\underline{F}^{\mathrm{r}}_{\mathrm{Q},m}\mathrm{e}^{\mathrm{j}m\varphi}\right) \end{aligned}. \qquad (10)$$

Distribution of MMF produced by the field winding current is expressed as

$$F^{\mathrm{r}}_{\mathrm{f},p}(\varphi) = \mathrm{Re}\left\{\left(\frac{N_{\mathrm{f}}}{2p}i^{\mathrm{r}}_{\mathrm{f},p}\right)\cdot \mathrm{e}^{\mathrm{j}p\varphi}\right\} = \mathrm{Re}\left(F^{\mathrm{r}}_{\mathrm{f},p}\cdot \mathrm{e}^{\mathrm{j}p\varphi}\right) = \mathrm{Re}\left(\underline{F}^{\mathrm{r}}_{\mathrm{f},p}\right). \qquad (11)$$

As it was already mentioned before, the MMF of the field winding is not sinusoidally distributed but rather constant over the rotor pole. On the other hand side, the air gap length over the pole-shoe is varying and so is the air gap permeance. This is done for the purpose to achieve the sinusoidal distribution of the magnetic flux density produced by the field winding. In this work, we have used a sinusoidal distribution of the field winding MMF and a constant air gap length (if no eccentricity is present) instead of actual constant MMF and varying air gap length. It can be shown that both approaches provide very similar distributions of the magnetic flux density in the air gap.

Total MMFs acting on d- and q-axis are

$$F_{\mathrm{dt}}^{\mathrm{r}}(\varphi)=\mathrm{Re}\left\{\left(F_{\mathrm{d},p}^{\mathrm{r}}+F_{\mathrm{f},p}^{\mathrm{r}}\right)\mathrm{e}^{\mathrm{j}p\varphi}+\sum_{\substack{m=1\\ m\neq p}}^{N_{\max}}\underline{F}_{\mathrm{D},m}^{\mathrm{r}}\mathrm{e}^{\mathrm{j}m\varphi}\right\}$$
$$F_{\mathrm{qt}}^{\mathrm{r}}(\varphi)=\mathrm{Re}\left\{F_{\mathrm{q},p}^{\mathrm{r}}\mathrm{e}^{\mathrm{j}p\varphi}+\sum_{\substack{m=1\\ m\neq p}}^{N_{\max}}\underline{F}_{\mathrm{Q},m}^{\mathrm{r}}\mathrm{e}^{\mathrm{j}m\varphi}\right\}. \qquad (12)$$

2.3 Air gap permeance with eccentric rotor

For a cylindrical stator with cylindrical but eccentrically placed rotor the radial air gap length can be fairly accurately approximated as

$$\delta^{\mathrm{r}}(\varphi)=\delta_0-\mathrm{Re}\left(\underline{\delta}_{\mathrm{ecc}}^{\mathrm{r}}\mathrm{e}^{\mathrm{j}\varphi}\right), \qquad (13)$$

here, δ_0 is the effective air gap length including the effects of slotting and saturation, $\underline{\delta}_{\mathrm{ecc}}^{\mathrm{r}}(\varphi)=\delta_{\mathrm{ecc}}\mathrm{e}^{\mathrm{j}\{-(\omega_{\mathrm{ecc}}-\omega_{\mathrm{m}})t+\varphi_{\mathrm{ecc.0}}\}}$ is the position of the rotor axis displacement (eccentric rotor shift) with respect to the coordinate system origin, $\delta_{\mathrm{ecc.}}$ is the whirling radius (eccentricity magnitude), $\omega_{\mathrm{ecc.}}$ is the whirling angular velocity, $\varphi_{\mathrm{ecc.0}}$ is the initial phase angle of the rotor displacement.

Air gap variation due to the rotor saliency can be modelled by applying different values of δ_0 to the effective air gap length on d- and q-axis. Thus, we have

$$\delta_{\mathrm{d}}^{\mathrm{r}}(\varphi)=\delta_{0,\mathrm{d}}-\mathrm{Re}\left(\underline{\delta}_{\mathrm{ecc}}^{\mathrm{r}}\mathrm{e}^{\mathrm{j}\varphi}\right)$$
$$\delta_{\mathrm{q}}^{\mathrm{r}}(\varphi)=\delta_{0,\mathrm{q}}-\mathrm{Re}\left(\underline{\delta}_{\mathrm{ecc}}^{\mathrm{r}}\mathrm{e}^{\mathrm{j}\left(\varphi+\frac{\pi}{2p}\right)}\right), \qquad (14)$$

here, $\delta_{0,\mathrm{d}}<\delta_{0,\mathrm{q}}$, and $\frac{\pi}{2p}$ is the angle between the d- and q-axis.

Air gap permeance per unit area is expressed as

$$\lambda(\varphi)=\frac{\mu_0}{\delta(\varphi)}, \qquad (15)$$

here, $\mu_0=4\pi\cdot10^{-7}$ is the permeability of an empty space.

Neglecting the higher order components the air gap permeance can be written

$$\lambda_{0,\mathrm{d}}^{\mathrm{r}}(\varphi)=\frac{\mu_0}{\delta_{0,\mathrm{d}}}\left(1+\frac{1}{\delta_{0,\mathrm{d}}}\mathrm{Re}\left(\underline{\delta}_{\mathrm{ecc.}}^{\mathrm{r}}\mathrm{e}^{\mathrm{j}\varphi}\right)\right)$$
$$\lambda_{0,\mathrm{q}}^{\mathrm{r}}(\varphi)=\frac{\mu_0}{\delta_{0,\mathrm{q}}}\left(1+\frac{1}{\delta_{0,\mathrm{q}}}\mathrm{Re}\left(\underline{\delta}_{\mathrm{ecc.}}^{\mathrm{r}}\mathrm{e}^{\mathrm{j}\left\{\varphi+\frac{\pi}{2p}\right\}}\right)\right). \qquad (16)$$

2.4 Magnetic flux density in the air gap

Magnetic flux density distribution in the air gap is obtained by multiplying the MMF by the corresponding air gap permeance

$$B_{\mathrm{dt}}^{\mathrm{r}}(\varphi)=F_{\mathrm{dt}}^{\mathrm{r}}(\varphi)\cdot\lambda_{0,\mathrm{d}}^{\mathrm{r}}(\varphi)$$
$$B_{\mathrm{qt}}^{\mathrm{r}}(\varphi)=F_{\mathrm{qt}}^{\mathrm{r}}(\varphi)\cdot\lambda_{0,\mathrm{q}}^{\mathrm{r}}(\varphi). \qquad (17)$$

Thus, the magnetic flux density on d-axis is

$$\begin{aligned}
B_{\mathrm{dt}}^{\mathrm{r}}(\varphi)=\frac{\mu_0}{\delta_{0,\mathrm{d}}}\mathrm{Re}\Bigg[&\left\{\left(F_{\mathrm{d},p}^{\mathrm{r}}+F_{\mathrm{f},p}^{\mathrm{r}}\right)+\frac{1}{2\delta_{0,\mathrm{d}}}\left(\underline{F}_{\mathrm{D},p-1}^{\mathrm{r}}\underline{\delta}_{\mathrm{ecc.}}^{\mathrm{r}}+\underline{F}_{\mathrm{D},p+1}^{\mathrm{r}}\underline{\delta}_{\mathrm{ecc.}}^{\mathrm{r}\,*}\right)\right\}\mathrm{e}^{\mathrm{j}p\varphi}+\\
&+\left\{\frac{\underline{\delta}_{\mathrm{ecc.}}^{\mathrm{r}\,*}}{2\delta_{0,\mathrm{d}}}\left(F_{\mathrm{d},p}^{\mathrm{r}}+F_{\mathrm{f},p}^{\mathrm{r}}\right)+\underline{F}_{\mathrm{D},p-1}^{\mathrm{r}}\right\}\mathrm{e}^{\mathrm{j}(p-1)\varphi}+\\
&+\left\{\frac{\underline{\delta}_{\mathrm{ecc.}}^{\mathrm{r}}}{2\delta_{0,\mathrm{d}}}\left(F_{\mathrm{d},p}^{\mathrm{r}}+F_{\mathrm{f},p}^{\mathrm{r}}\right)+\underline{F}_{\mathrm{D},p+1}^{\mathrm{r}}\right\}\mathrm{e}^{\mathrm{j}(p+1)\varphi}+\\
&+\sum_{\substack{m=1\\ m\neq p\neq p\pm1}}^{N_{\max}}\underline{F}_{\mathrm{D},m}^{\mathrm{r}}\left\{\mathrm{e}^{\mathrm{j}m\varphi}+\frac{1}{2\delta_{0,\mathrm{d}}}\left(\underline{\delta}_{\mathrm{ecc.}}^{\mathrm{r}}\mathrm{e}^{\mathrm{j}(m+1)\varphi}+\underline{\delta}_{\mathrm{ecc.}}^{\mathrm{r}\,*}\mathrm{e}^{\mathrm{j}(m-1)\varphi}\right)\right\}+\\
&+\frac{1}{2\delta_{0,\mathrm{d}}}\left(\underline{F}_{\mathrm{D},p-1}^{\mathrm{r}}\underline{\delta}_{\mathrm{ecc.}}^{\mathrm{r}\,*}\mathrm{e}^{\mathrm{j}(p-2)\varphi}+\underline{F}_{\mathrm{D},p+1}^{\mathrm{r}}\underline{\delta}_{\mathrm{ecc.}}^{\mathrm{r}}\mathrm{e}^{\mathrm{j}(p+2)\varphi}\right)\Bigg]
\end{aligned}, \qquad (18)$$

here, symbol " * " is used to denote the complex conjugate.

The fundamental components of the MMF are assumed to be preponderant. Due to their large magnitude the $p \pm 1$ MMF harmonics produced by the damper winding currents have also to be taken into account. The rest of the MMF harmonics are neglected hereafter. Thus, the magnetic flux density on d-axis is

$$B_{\mathrm{dt}}^{\mathrm{r}}(\varphi)=\mathrm{Re}\left(B_{\mathrm{dt},p}^{\mathrm{r}}\mathrm{e}^{\mathrm{j}p\varphi}+\underline{B}_{\mathrm{dt},p-1}^{\mathrm{r}}\mathrm{e}^{\mathrm{j}(p-1)\varphi}+\underline{B}_{\mathrm{dt},p+1}^{\mathrm{r}}\mathrm{e}^{\mathrm{j}(p+1)\varphi}\right), \qquad (19)$$

here, the components are

$$
\begin{aligned}
B^{\mathrm{r}}_{\mathrm{dt},\,p} &= \frac{\mu_0}{\delta_{0,\mathrm{d}}}\left(F^{\mathrm{r}}_{\mathrm{d},\,p} + F^{\mathrm{r}}_{\mathrm{f},\,p}\right) \\
\underline{B}^{\mathrm{r}}_{\mathrm{dt},\,p-1} &= \frac{\mu_0}{\delta_{0,\mathrm{d}}}\left[\frac{\underline{\delta}^{\mathrm{r}\,*}_{\mathrm{ecc.}}}{2\delta_{0,\mathrm{d}}}\left(F^{\mathrm{r}}_{\mathrm{d},\,p} + F^{\mathrm{r}}_{\mathrm{f},\,p}\right) + \underline{F}^{\mathrm{r}}_{\mathrm{D},\,p-1}\right]. \qquad (20) \\
\underline{B}^{\mathrm{r}}_{\mathrm{dt},\,p+1} &= \frac{\mu_0}{\delta_{0,\mathrm{d}}}\left[\frac{\underline{\delta}^{\mathrm{r}}_{\mathrm{ecc.}}}{2\delta_{0,\mathrm{d}}}\left(F^{\mathrm{r}}_{\mathrm{d},\,p} + F^{\mathrm{r}}_{\mathrm{f},\,p}\right) + \underline{F}^{\mathrm{r}}_{\mathrm{D},\,p+1}\right]
\end{aligned}
$$

Similarly, the magnetic flux density on q-axis is

$$
\begin{aligned}
B^{\mathrm{r}}_{\mathrm{qt}}(\varphi) = \frac{\mu_0}{\delta_{0,\mathrm{q}}}\mathrm{Re}\Bigg[&\left\{F^{\mathrm{r}}_{\mathrm{q},\,p} + \frac{1}{2\delta_{0,\mathrm{q}}}\left(\underline{F}^{\mathrm{r}}_{\mathrm{Q},\,p-1}\underline{\delta}^{\mathrm{r}}_{\mathrm{ecc.}}\mathrm{e}^{\mathrm{j}\frac{\pi}{2p}} + \underline{F}^{\mathrm{r}}_{\mathrm{Q},\,p+1}\underline{\delta}^{\mathrm{r}\,*}_{\mathrm{ecc.}}\mathrm{e}^{-\mathrm{j}\frac{\pi}{2p}}\right)\right\}\mathrm{e}^{\mathrm{j}p\varphi} + \\
&+\left(\frac{\underline{\delta}^{\mathrm{r}\,*}_{\mathrm{ecc.}}}{2\delta_{0,\mathrm{q}}}F^{\mathrm{r}}_{\mathrm{q},\,p}\mathrm{e}^{-\mathrm{j}\frac{\pi}{2p}} + \underline{F}^{\mathrm{r}}_{\mathrm{Q},\,p-1}\right)\mathrm{e}^{\mathrm{j}(p-1)\varphi} + \\
&+\left(\frac{\underline{\delta}^{\mathrm{r}}_{\mathrm{ecc.}}}{2\delta_{0,\mathrm{q}}}F^{\mathrm{r}}_{\mathrm{q},\,p}\mathrm{e}^{\mathrm{j}\frac{\pi}{2p}} + \underline{F}^{\mathrm{r}}_{\mathrm{Q},\,p+1}\right)\mathrm{e}^{\mathrm{j}(p+1)\varphi} + \qquad . \quad (21) \\
&+\sum_{\substack{m=1\\ m\neq p\neq p\pm 1}}^{N_{\max}}\underline{F}^{\mathrm{r}}_{\mathrm{Q},\,m}\left(\mathrm{e}^{\mathrm{j}m\varphi} + \frac{1}{2\delta_{0,\mathrm{q}}}\left[\underline{\delta}^{\mathrm{r}}_{\mathrm{ecc.}}\mathrm{e}^{\mathrm{j}\left\{(m+1)\varphi+\frac{\pi}{2p}\right\}} + \underline{\delta}^{\mathrm{r}\,*}_{\mathrm{ecc.}}\mathrm{e}^{\mathrm{j}\left\{(m-1)\varphi-\frac{\pi}{2p}\right\}}\right]\right) + \\
&+\frac{1}{2\delta_{0,\mathrm{q}}}\left(\underline{F}^{\mathrm{r}}_{\mathrm{Q},\,p-1}\underline{\delta}^{\mathrm{r}\,*}_{\mathrm{ecc.}}\mathrm{e}^{\mathrm{j}\left\{(p-2)-\frac{\pi}{2p}\right\}} + \underline{F}^{\mathrm{r}}_{\mathrm{Q},\,p+1}\underline{\delta}^{\mathrm{r}}_{\mathrm{ecc.}}\mathrm{e}^{\mathrm{j}\left\{(p+2)+\frac{\pi}{2p}\right\}}\right)\Bigg]
\end{aligned}
$$

Applying the simplifying assumptions yields

$$
B^{\mathrm{r}}_{\mathrm{qt}}(\varphi) = \mathrm{Re}\left(B^{\mathrm{r}}_{\mathrm{qt},\,p}\mathrm{e}^{\mathrm{j}p\varphi} + \underline{B}^{\mathrm{r}}_{\mathrm{qt},\,p-1}\mathrm{e}^{\mathrm{j}(p-1)\varphi} + \underline{B}^{\mathrm{r}}_{\mathrm{qt},\,p+1}\mathrm{e}^{\mathrm{j}(p+1)\varphi}\right), \qquad (22)
$$

here, the components are

$$
\begin{aligned}
B^{\mathrm{r}}_{\mathrm{qt},\,p} &= \frac{\mu_0}{\delta_{0,\mathrm{q}}}F^{\mathrm{r}}_{\mathrm{q},\,p} \\
\underline{B}^{\mathrm{r}}_{\mathrm{qt},\,p-1} &= \frac{\mu_0}{\delta_{0,\mathrm{q}}}\left[\frac{\underline{\delta}^{\mathrm{r}\,*}_{\mathrm{ecc.}}}{2\delta_{0,\mathrm{q}}}F^{\mathrm{r}}_{\mathrm{q},\,p}\mathrm{e}^{-\mathrm{j}\frac{\pi}{2p}} + \underline{F}^{\mathrm{r}}_{\mathrm{Q},\,p-1}\right]. \qquad (23) \\
\underline{B}^{\mathrm{r}}_{\mathrm{qt},\,p+1} &= \frac{\mu_0}{\delta_{0,\mathrm{q}}}\left[\frac{\underline{\delta}^{\mathrm{r}}_{\mathrm{ecc.}}}{2\delta_{0,\mathrm{q}}}F^{\mathrm{r}}_{\mathrm{q},\,p}\mathrm{e}^{\mathrm{j}\frac{\pi}{2p}} + \underline{F}^{\mathrm{r}}_{\mathrm{Q},\,p+1}\right]
\end{aligned}
$$

The total magnetic flux density can be considered as a sum of the magnetic flux densities on d- and q-axis. Thus, the spatial distribution of the total magnetic flux density in the air gap is

$$\begin{aligned} B_{\mathrm{t}}^{\mathrm{r}}(\varphi) &= \mathrm{Re}\left(\underline{B}_{\mathrm{t},p}^{\mathrm{r}}(\varphi) + \underline{B}_{\mathrm{t},p-1}^{\mathrm{r}}(\varphi) + \underline{B}_{\mathrm{t},p+1}^{\mathrm{r}}(\varphi)\right) = \\ &\mathrm{Re}\Big[\left(B_{\mathrm{dt},p}^{\mathrm{r}} + \mathrm{j}B_{\mathrm{qt},p}^{\mathrm{r}}\right)\mathrm{e}^{\mathrm{j}p\varphi} + \left(\underline{B}_{\mathrm{dt},p-1}^{\mathrm{r}} + \mathrm{j}\underline{B}_{\mathrm{qt},p-1}^{\mathrm{r}}\right)\mathrm{e}^{\mathrm{j}(p-1)\varphi} + \\ &+\left(\underline{B}_{\mathrm{dt},p+1}^{\mathrm{r}} + \mathrm{j}\underline{B}_{\mathrm{qt},p+1}^{\mathrm{r}}\right)\mathrm{e}^{\mathrm{j}(p+1)\varphi}\Big] \end{aligned} \quad (24)$$

The flux density components can also be expressed in terms of the fundamental field and current harmonics

$$\begin{aligned} B_{\mathrm{dt},p}^{\mathrm{r}} &= \frac{\mu_0}{\delta_{0,\mathrm{d}}}\left[\frac{3}{2}\frac{N_{\mathrm{se}}}{2p} i_{\mathrm{d},p}^{\mathrm{r}} + \frac{N_{\mathrm{f}}}{2p} i_{\mathrm{f},p}^{\mathrm{r}}\right] \\ \underline{B}_{\mathrm{dt},p-1}^{\mathrm{r}} &= \frac{\underline{\delta}_{\mathrm{ecc.}}^{\mathrm{r}\,*}}{2\delta_{0,\mathrm{d}}} B_{\mathrm{dt},p}^{\mathrm{r}} + \frac{\mu_0}{\delta_{0,\mathrm{d}}} k_{\mathrm{D},p-1}\underline{i}_{\mathrm{D},p-1}^{\mathrm{r}}, \\ \underline{B}_{\mathrm{dt},p+1}^{\mathrm{r}} &= \frac{\underline{\delta}_{\mathrm{ecc.}}^{\mathrm{r}}}{2\delta_{0,\mathrm{d}}} B_{\mathrm{dt},p}^{\mathrm{r}} + \frac{\mu_0}{\delta_{0,\mathrm{d}}} k_{\mathrm{D},p+1}\underline{i}_{\mathrm{D},p+1}^{\mathrm{r}} \end{aligned} \quad (25)$$

here, $k_{\mathrm{D},p\pm1}$ are the additional coupling factors due to the leakage flux and saturation [15].

Similar expressions can also be written for the q-axis magnetic flux density components

$$\begin{aligned} B_{\mathrm{qt},p}^{\mathrm{r}} &= \frac{3}{2}\frac{N_{\mathrm{se}}}{2p}\frac{\mu_0}{\delta_{0,\mathrm{q}}} i_{\mathrm{q},p}^{\mathrm{r}} \\ \underline{B}_{\mathrm{qt},p-1}^{\mathrm{r}} &= \frac{\underline{\delta}_{\mathrm{ecc.}}^{\mathrm{r}\,*}}{2\delta_{0,\mathrm{q}}} B_{\mathrm{qt},p}^{\mathrm{r}}\mathrm{e}^{-\mathrm{j}\frac{\pi}{2p}} + \frac{\mu_0}{\delta_{0,\mathrm{q}}} k_{\mathrm{Q},p-1}\underline{i}_{\mathrm{Q},p-1}^{\mathrm{r}}. \\ \underline{B}_{\mathrm{qt},p+1}^{\mathrm{r}} &= \frac{\underline{\delta}_{\mathrm{ecc.}}^{\mathrm{r}}}{2\delta_{0,\mathrm{q}}} B_{\mathrm{qt},p}^{\mathrm{r}}\mathrm{e}^{\mathrm{j}\frac{\pi}{2p}} + \frac{\mu_0}{\delta_{0,\mathrm{q}}} k_{\mathrm{Q},p+1}\underline{i}_{\mathrm{Q},p+1}^{\mathrm{r}} \end{aligned} \quad (26)$$

Thus, combining equations (24), (25) and (26) yields

$$
\begin{aligned}
&\mathrm{Re}\left(\underline{B}^{\mathrm{r}}_{\mathrm{t},\,p}(\varphi)\right)=\frac{B^{\mathrm{r}}_{\mathrm{dt},\,p}}{2}\left(\mathrm{e}^{\mathrm{j}\,p\varphi}+\mathrm{e}^{-\mathrm{j}\,p\varphi}\right)+\frac{\mathrm{j}B^{\mathrm{r}}_{\mathrm{qt},\,p}}{2}\left(\mathrm{e}^{\mathrm{j}\,p\varphi}-\mathrm{e}^{-\mathrm{j}\,p\varphi}\right)\\
&\mathrm{Re}\left(\underline{B}^{\mathrm{r}}_{\mathrm{t},\,p-1}(\varphi)\right)=\frac{1}{2}\frac{B^{\mathrm{r}}_{\mathrm{dt},\,p}}{2\delta_{0,\mathrm{d}}}\left(\underline{\delta}^{\mathrm{r}}_{\mathrm{ecc.}}{}^{*}\mathrm{e}^{\mathrm{j}(p-1)\varphi}+\underline{\delta}^{\mathrm{r}}_{\mathrm{ecc.}}\mathrm{e}^{-\mathrm{j}(p-1)\varphi}\right)+\\
&+\frac{\mu_0}{2\delta_{0,\mathrm{d}}}k_{\mathrm{D},\,p-1}\left(\underline{i}^{\mathrm{r}}_{\mathrm{D},\,p-1}\mathrm{e}^{\mathrm{j}(p-1)\varphi}+\underline{i}^{\mathrm{r}}_{\mathrm{D},\,p-1}{}^{*}\mathrm{e}^{-\mathrm{j}(p-1)\varphi}\right)+\\
&+\mathrm{j}\frac{1}{2}\frac{B^{\mathrm{r}}_{\mathrm{qt},\,p}}{2\delta_{0,\mathrm{q}}}\left(\underline{\delta}^{\mathrm{r}}_{\mathrm{ecc.}}{}^{*}\mathrm{e}^{-\mathrm{j}\frac{\pi}{2p}}\mathrm{e}^{\mathrm{j}(p-1)\varphi}-\underline{\delta}^{\mathrm{r}}_{\mathrm{ecc.}}\mathrm{e}^{\mathrm{j}\frac{\pi}{2p}}\mathrm{e}^{-\mathrm{j}(p-1)\varphi}\right)+\\
&+\mathrm{j}\frac{\mu_0}{2\delta_{0,\mathrm{q}}}k_{\mathrm{Q},\,p-1}\left(\underline{i}^{\mathrm{r}}_{\mathrm{Q},\,p-1}\mathrm{e}^{\mathrm{j}(p-1)\varphi}-\underline{i}^{\mathrm{r}}_{\mathrm{Q},\,p-1}{}^{*}\mathrm{e}^{-\mathrm{j}(p-1)\varphi}\right)\\
&\mathrm{Re}\left(\underline{B}^{\mathrm{r}}_{\mathrm{t},\,p+1}(\varphi)\right)=\frac{1}{2}\frac{B^{\mathrm{r}}_{\mathrm{dt},\,p}}{2\delta_{0,\mathrm{d}}}\left(\underline{\delta}^{\mathrm{r}}_{\mathrm{ecc.}}\mathrm{e}^{\mathrm{j}(p+1)\varphi}+\underline{\delta}^{\mathrm{r}}_{\mathrm{ecc.}}{}^{*}\mathrm{e}^{-\mathrm{j}(p+1)\varphi}\right)+\\
&+\frac{\mu_0}{2\delta_{0,\mathrm{d}}}k_{\mathrm{D},\,p+1}\left(\underline{i}^{\mathrm{r}}_{\mathrm{D},\,p+1}\mathrm{e}^{\mathrm{j}(p+1)\varphi}+\underline{i}^{\mathrm{r}}_{\mathrm{D},\,p+1}{}^{*}\mathrm{e}^{-\mathrm{j}(p+1)\varphi}\right)+\\
&+\mathrm{j}\frac{1}{2}\frac{B^{\mathrm{r}}_{\mathrm{qt},\,p}}{2\delta_{0,\mathrm{q}}}\left(\underline{\delta}^{\mathrm{r}}_{\mathrm{ecc.}}\mathrm{e}^{\mathrm{j}\frac{\pi}{2p}}\mathrm{e}^{\mathrm{j}(p+1)\varphi}-\underline{\delta}^{\mathrm{r}}_{\mathrm{ecc.}}{}^{*}\mathrm{e}^{-\mathrm{j}\frac{\pi}{2p}}\mathrm{e}^{-\mathrm{j}(p+1)\varphi}\right)+\\
&+\mathrm{j}\frac{\mu_0}{2\delta_{0,\mathrm{q}}}k_{\mathrm{Q},\,p+1}\left(\underline{i}^{\mathrm{r}}_{\mathrm{Q},\,p+1}\mathrm{e}^{\mathrm{j}(p+1)\varphi}-\underline{i}^{\mathrm{r}}_{\mathrm{Q},\,p+1}{}^{*}\mathrm{e}^{-\mathrm{j}(p+1)\varphi}\right)
\end{aligned}
\quad . \qquad (27)
$$

2.5 Rotor cage fluxes

Rotor cage fluxes of the orders $p \pm 1$ acting on d- and q-axis can be expressed as

$$
\underline{\phi}^{\mathrm{r}}_{\mathrm{D},\,p-1}=L_{\mathrm{D},p-1}\left(\frac{\underline{\delta}^{\mathrm{r}}_{\mathrm{ecc.}}{}^{*}k_{\mathrm{D},\,p-1}}{2\mu_0}B^{\mathrm{r}}_{\mathrm{dt},\,p}+\underline{i}^{\mathrm{r}}_{\mathrm{D},\,p-1}\right)\qquad \underline{\phi}^{\mathrm{r}}_{\mathrm{D},\,p+1}=L_{\mathrm{D},p+1}\left(\frac{\underline{\delta}^{\mathrm{r}}_{\mathrm{ecc.}}k_{\mathrm{D},\,p+1}}{2\mu_0}B^{\mathrm{r}}_{\mathrm{dt},\,p}+\underline{i}^{\mathrm{r}}_{\mathrm{D},\,p+1}\right)
$$

$$
\underline{\phi}^{\mathrm{r}}_{\mathrm{Q},\,p-1}=L_{\mathrm{Q},p-1}\left(\frac{\underline{\delta}^{\mathrm{r}}_{\mathrm{ecc.}}{}^{*}\mathrm{e}^{-\mathrm{j}\frac{\pi}{2p}}k_{\mathrm{Q},\,p-1}}{2\mu_0}B^{\mathrm{r}}_{\mathrm{qt},\,p}+\underline{i}^{\mathrm{r}}_{\mathrm{Q},\,p-1}\right)\qquad \underline{\phi}^{\mathrm{r}}_{\mathrm{Q},\,p+1}=L_{\mathrm{Q},p+1}\left(\frac{\underline{\delta}^{\mathrm{r}}_{\mathrm{ecc.}}\mathrm{e}^{\mathrm{j}\frac{\pi}{2p}}k_{\mathrm{Q},\,p+1}}{2\mu_0}B^{\mathrm{r}}_{\mathrm{qt},\,p}+\underline{i}^{\mathrm{r}}_{\mathrm{Q},\,p+1}\right)
\quad , (28)
$$

here, $L_{\mathrm{D},p\pm1}$ and $L_{\mathrm{Q},p\pm1}$ are the self-inductances of the rotor cage mesh on the corresponding axes.

2.6 Voltage equations for the rotor cage

For $p \pm 1$ voltage harmonics in the rotor cage we can write

$$L_{\mathrm{D}\sigma,p-1}\frac{\mathrm{d}\underline{i}^{\mathrm{r}}_{\mathrm{D},p-1}}{\mathrm{d}t}+R_{\mathrm{D},p-1}\underline{i}^{\mathrm{r}}_{\mathrm{D},p-1}+\frac{\mathrm{d}\underline{\phi}^{\mathrm{r}}_{\mathrm{D},p-1}}{\mathrm{d}t}=0 \quad L_{\mathrm{D}\sigma,p+1}\frac{\mathrm{d}\underline{i}^{\mathrm{r}}_{\mathrm{D},p+1}}{\mathrm{d}t}+R_{\mathrm{D},p+1}\underline{i}^{\mathrm{r}}_{\mathrm{D},p+1}+\frac{\mathrm{d}\underline{\phi}^{\mathrm{r}}_{\mathrm{D},p+1}}{\mathrm{d}t}=0$$
$$L_{\mathrm{Q}\sigma,p-1}\frac{\mathrm{d}\underline{i}^{\mathrm{r}}_{\mathrm{Q},p-1}}{\mathrm{d}t}+R_{\mathrm{Q},p-1}\underline{i}^{\mathrm{r}}_{\mathrm{Q},p-1}+\frac{\mathrm{d}\underline{\phi}^{\mathrm{r}}_{\mathrm{Q},p-1}}{\mathrm{d}t}=0 \quad L_{\mathrm{Q}\sigma,p+1}\frac{\mathrm{d}\underline{i}^{\mathrm{r}}_{\mathrm{Q},p+1}}{\mathrm{d}t}+R_{\mathrm{Q},p+1}\underline{i}_{\mathrm{Q},p+1}+\frac{\mathrm{d}\underline{\phi}^{\mathrm{r}}_{\mathrm{Q},p+1}}{\mathrm{d}t}=0, \tag{29}$$

here, $R_{\mathrm{D},p-1}, R_{\mathrm{D},p+1}, R_{\mathrm{Q},p-1}, R_{\mathrm{Q},p+1}$ consist of the damper bar and end-ring segments resistances for the corresponding current harmonics on the corresponding axes; $L_{\mathrm{D}\sigma,p-1}, L_{\mathrm{D}\sigma,p+1}, L_{\mathrm{Q}\sigma,p-1}, L_{\mathrm{Q}\sigma,p+1}$ take into account the effects of the slot- and tooth-tip leakage inductance of a damper bar and the end-leakage inductance of a ring segment for the corresponding harmonics on the corresponding axes.

2.7 Total magnetic force on the rotor

To calculate the electromagnetic force acting on the rotor we apply Maxwell stress tensor

$$\sigma^{\mathrm{r}}=\frac{1}{2\mu_0}\left[B^{\mathrm{r}}(\varphi)\right]^2=\frac{1}{2\mu_0}\left[\sum_{\upsilon=0}^{\infty}\mathrm{Re}\left\{\underline{B}^{\mathrm{r}}_{\upsilon}(\varphi)\mathrm{e}^{\mathrm{j}\upsilon\varphi}\right\}\right]^2. \tag{30}$$

The total electromagnetic force is obtained by integrating the Maxwell stress tensor over the whole circumferential length of a machine

$$\underline{F}^{\mathrm{r}}_{\mathrm{e}}=\frac{d_{\mathrm{r}}l_{\mathrm{e}}}{2}\int_0^{2\pi}\sigma^{\mathrm{r}}(\varphi)\cdot\mathrm{e}^{-\mathrm{j}\varphi}\,\mathrm{d}\varphi, \tag{31}$$

here d_{r} is the outer diameter of the rotor, l_{e} is the equivalent axial length of the machine.

Assuming that the force on the rotor is generated due to the product of two magnetic flux density harmonics we can write

$$\underline{F}^{\mathrm{r}}_{\mathrm{e}}=\frac{d_{\mathrm{r}}l_{\mathrm{e}}}{8\mu_0}\int_0^{2\pi}\left(\underline{B}^{\mathrm{r}}_{m}\underline{B}^{\mathrm{r}*}_{n}\mathrm{e}^{\mathrm{j}(m-n-1)\varphi}+\underline{B}^{\mathrm{r}*}_{m}\underline{B}^{\mathrm{r}}_{n}\mathrm{e}^{-\mathrm{j}(m-n+1)\varphi}\right)\mathrm{d}\varphi. \tag{32}$$

Thus, the net force acting on the rotor can only be produced by the magnetic flux density components with wave numbers satisfying the condition $m-n=\pm1$.

Rotor eccentricity mainly causes the magnetic flux components of the orders p, $p-1$ and $p+1$ (see equation (24)). Therefore, the total electromagnetic force in rotor frame of reference can be represented as

$$\underline{F}_{\mathrm{e}}^{\mathrm{r}} = \frac{\pi d_{\mathrm{r}} l_{\mathrm{e}}}{4\mu_0}\left[\left(\frac{{B_{\mathrm{dt},p}^{\mathrm{r}}}^{2}}{\delta_{0,\mathrm{d}}} + \frac{{B_{\mathrm{qt},p}^{\mathrm{r}}}^{2}}{\delta_{0,\mathrm{q}}}\mathrm{e}^{\mathrm{j}\frac{\pi}{2p}}\right)\underline{\delta}_{\mathrm{ecc.}}^{\mathrm{r}} + \frac{\mu_0}{\delta_{0,\mathrm{d}}}\left(k_{\mathrm{D},p-1}{\underline{i}_{\mathrm{D},p-1}^{\mathrm{r}}}^{*}\left\{B_{\mathrm{dt},p}^{\mathrm{r}} + \mathrm{j}B_{\mathrm{qt},p}^{\mathrm{r}}\right\} + \right.\right.$$

$$\left. + k_{\mathrm{D},p+1}\underline{i}_{\mathrm{D},p+1}^{\mathrm{r}}\left\{B_{\mathrm{dt},p}^{\mathrm{r}} - \mathrm{j}B_{\mathrm{qt},p}^{\mathrm{r}}\right\}\right) + \frac{\mu_0}{\delta_{0,\mathrm{q}}}\left(k_{\mathrm{Q},p-1}{\underline{i}_{\mathrm{Q},p-1}^{\mathrm{r}}}^{*}\left\{B_{\mathrm{qt},p}^{\mathrm{r}} - \mathrm{j}B_{\mathrm{dt},p}^{\mathrm{r}}\right\} + \right. \quad . \quad (33)$$

$$\left.\left. + k_{\mathrm{Q},p+1}\underline{i}_{\mathrm{Q},p+1}^{\mathrm{r}}\left\{B_{\mathrm{qt},p}^{\mathrm{r}} + \mathrm{j}B_{\mathrm{dt},p}^{\mathrm{r}}\right\}\right)\right]$$

This equation shows that there are several force components: firstly, there is a force component produced by the fundamental magnetic flux density waves and rotor eccentricity; secondly, there are force components due to the interactions of the fundamental magnetic field and $p \pm 1$ current harmonics on d-axis; and finally, there are force components due to the interactions of the fundamental magnetic field and $p \pm 1$ current harmonics on q-axis. Since the effective air gap length on d-axis is substantially smaller than that on q-axis ($\delta_{0,\mathrm{d}} < \delta_{0,\mathrm{q}}$) and the rotor cage currents on d-axis are stronger than those on q-axis, it would be reasonable to assume that the force component $\frac{\pi d_{\mathrm{r}} l_{\mathrm{e}}}{4\delta_{0,\mathrm{d}}}\left(\left\{B_{\mathrm{dt},p}^{\mathrm{r}} + \mathrm{j}B_{\mathrm{qt},p}^{\mathrm{r}}\right\}k_{\mathrm{D},p-1}{\underline{i}_{\mathrm{D},p-1}^{\mathrm{r}}}^{*} + \left\{B_{\mathrm{dt},p}^{\mathrm{r}} - \mathrm{j}B_{\mathrm{qt},p}^{\mathrm{r}}\right\}k_{\mathrm{D},p+1}\underline{i}_{\mathrm{D},p+1}^{\mathrm{r}}\right)$ is considerably stronger than $\frac{\pi d_{\mathrm{r}} l_{\mathrm{e}}}{4\delta_{0,\mathrm{q}}}\left(\left\{B_{\mathrm{qt},p}^{\mathrm{r}} - \mathrm{j}B_{\mathrm{dt},p}^{\mathrm{r}}\right\}k_{\mathrm{Q},p-1}{\underline{i}_{\mathrm{Q},p-1}^{\mathrm{r}}}^{*} + \left\{B_{\mathrm{qt},p}^{\mathrm{r}} + \mathrm{j}B_{\mathrm{dt},p}^{\mathrm{r}}\right\}k_{\mathrm{Q},p+1}\underline{i}_{\mathrm{Q},p+1}^{\mathrm{r}}\right)$.

2.8 Circular whirling of the rotor during the operation at a constant flux

Circular whirling of the rotor is described as the rotor axis motion about the stator bore axis at a constant distance with a certain angular speed. Mathematically this is expressed as

$$\underline{\delta}_{\mathrm{ecc}}^{\mathrm{r}}(\varphi) = \delta_{\mathrm{ecc}}\mathrm{e}^{\mathrm{j}\left\{-(\omega_{\mathrm{ecc}}-\omega_{\mathrm{m}})t+\varphi_{\mathrm{ecc.0}}\right\}} = \delta_{\mathrm{ecc.}}\mathrm{e}^{\mathrm{j}\left\{-\omega_{\mathrm{ecc.}}^{\mathrm{r}}t+\varphi_{\mathrm{ecc.0}}\right\}}. \qquad (34)$$

Operation at a constant flux assumes that the fundamental fluxes on d- and q-axis have constant magnitudes and are stationary in the rotor frame of reference

$$\begin{aligned} B_{\mathrm{dt},p}^{\mathrm{r}} &= B_{\mathrm{dt},p} = \mathrm{const} \\ B_{\mathrm{qt},p}^{\mathrm{r}} &= B_{\mathrm{qt},p} = \mathrm{const} \end{aligned} . \quad (35)$$

It is also assumed that the fundamental components of the magnetic flux density are not affected by the eccentric rotor motion.

The total electromagnetic force acting on the rotor of a machine is described by equation (33). In this equation, the current harmonics of the rotor cage can be expressed in terms of the fundamental magnetic flux density components and rotor eccentricity. For this purpose, equation (28) is substituted into equation (29) yielding

$$
\begin{aligned}
&L_{\mathrm{Dt},p-1}\frac{\mathrm{d}\underline{i}^{\mathrm{r}}_{\mathrm{D},p-1}}{\mathrm{d}t}+R_{\mathrm{D},p-1}\underline{i}^{\mathrm{r}}_{\mathrm{D},p-1}+\frac{k_{\mathrm{D},p-1}L_{\mathrm{D},p-1}}{2\mu_0}\frac{\mathrm{d}}{\mathrm{d}t}\left(\underline{\delta}^{\mathrm{r}}_{\mathrm{ecc.}}{}^{*}B^{\mathrm{r}}_{\mathrm{dt},p}\right)=0\\
&L_{\mathrm{Qt},p-1}\frac{\mathrm{d}\underline{i}^{\mathrm{r}}_{\mathrm{Q},p-1}}{\mathrm{d}t}+R_{\mathrm{Q},p-1}\underline{i}^{\mathrm{r}}_{\mathrm{Q},p-1}+\frac{k_{\mathrm{Q},p-1}L_{\mathrm{Q},p-1}\mathrm{e}^{-\mathrm{j}\frac{\pi}{2p}}}{2\mu_0}\frac{\mathrm{d}}{\mathrm{d}t}\left(\underline{\delta}^{\mathrm{r}}_{\mathrm{ecc.}}{}^{*}B^{\mathrm{r}}_{\mathrm{qt},p}\right)=0\\
&L_{\mathrm{Dt},p+1}\frac{\mathrm{d}\underline{i}^{\mathrm{r}}_{\mathrm{D},p+1}}{\mathrm{d}t}+R_{\mathrm{D},p+1}\underline{i}^{\mathrm{r}}_{\mathrm{D},p+1}+\frac{k_{\mathrm{D},p+1}L_{\mathrm{D},p+1}}{2\mu_0}\frac{\mathrm{d}}{\mathrm{d}t}\left(\underline{\delta}^{\mathrm{r}}_{\mathrm{ecc.}}B^{\mathrm{r}}_{\mathrm{dt},p}\right)=0\\
&L_{\mathrm{Qt},p+1}\frac{\mathrm{d}\underline{i}^{\mathrm{r}}_{\mathrm{Q},p+1}}{\mathrm{d}t}+R_{\mathrm{Q},p+1}\underline{i}_{\mathrm{Q},p+1}+\frac{k_{\mathrm{Q},p+1}L_{\mathrm{Q},p+1}\mathrm{e}^{\mathrm{j}\frac{\pi}{2p}}}{2\mu_0}\frac{\mathrm{d}}{\mathrm{d}t}\left(\underline{\delta}^{\mathrm{r}}_{\mathrm{ecc.}}B^{\mathrm{r}}_{\mathrm{qt},p}\right)=0
\end{aligned}
\quad , \qquad (36)
$$

here, $L_{\mathrm{Dt},p-1}=L_{\mathrm{D}\sigma,p-1}+L_{\mathrm{D},p-1}$, $L_{\mathrm{Qt},p-1}=L_{\mathrm{Q}\sigma,p-1}+L_{\mathrm{Q},p-1}$, $L_{\mathrm{Dt},p+1}=L_{\mathrm{D}\sigma,p+1}+L_{\mathrm{D},p+1}$ and $L_{\mathrm{Qt},p+1}=L_{\mathrm{Q}\sigma,p+1}+L_{\mathrm{Q},p+1}$ are the total harmonic inductances associated with d- and q-axis.

Using this system of equations the rotor cage currents $\underline{i}^{\mathrm{r}}_{\mathrm{D},p-1}$, $\underline{i}^{\mathrm{r}}_{\mathrm{Q},p-1}$, $\underline{i}^{\mathrm{r}}_{\mathrm{D},p+1}$ and $\underline{i}^{\mathrm{r}}_{\mathrm{Q},p+1}$ are solved

$$
\begin{aligned}
&\underline{i}^{\mathrm{r}}_{\mathrm{D},p-1}=\frac{k_{\mathrm{D},p-1}L_{\mathrm{D},p-1}B^{\mathrm{r}}_{\mathrm{dt},p}\delta^{\mathrm{r}}_{\mathrm{ecc.}}{}^{*}}{2\mu_0 L_{\mathrm{Dt},p-1}}\left(-1+\frac{1}{1+\mathrm{j}\omega^{\mathrm{r}}_{\mathrm{ecc.}}\left\{L_{\mathrm{Dt},p-1}/R_{\mathrm{D},p-1}\right\}}\right)\mathrm{e}^{\mathrm{j}\omega^{\mathrm{r}}_{\mathrm{ecc.}}t}\\
&\underline{i}^{\mathrm{r}}_{\mathrm{Q},p-1}=\frac{k_{\mathrm{Q},p-1}L_{\mathrm{Q},p-1}\mathrm{e}^{-\mathrm{j}\frac{\pi}{2p}}B^{\mathrm{r}}_{\mathrm{qt},p}\delta^{\mathrm{r}}_{\mathrm{ecc.}}{}^{*}}{2\mu_0 L_{\mathrm{Qt},p-1}}\left(-1+\frac{1}{1+\mathrm{j}\omega^{\mathrm{r}}_{\mathrm{ecc.}}\left\{L_{\mathrm{Qt},p-1}/R_{\mathrm{Q},p-1}\right\}}\right)\mathrm{e}^{\mathrm{j}\omega^{\mathrm{r}}_{\mathrm{ecc.}}t}\\
&\underline{i}^{\mathrm{r}}_{\mathrm{D},p+1}=\frac{k_{\mathrm{D},p+1}L_{\mathrm{D},p+1}B^{\mathrm{r}}_{\mathrm{dt},p}\delta^{\mathrm{r}}_{\mathrm{ecc.}}}{2\mu_0 L_{\mathrm{Dt},p+1}}\left(-1+\frac{1}{1-\mathrm{j}\omega^{\mathrm{r}}_{\mathrm{ecc.}}\left(L_{\mathrm{Dt},p+1}/R_{\mathrm{D},p+1}\right)}\right)\mathrm{e}^{-\mathrm{j}\omega^{\mathrm{r}}_{\mathrm{ecc.}}t}\\
&\underline{i}_{\mathrm{Q},p+1}=\frac{k_{\mathrm{Q},p+1}L_{\mathrm{Q},p+1}\mathrm{e}^{\mathrm{j}\frac{\pi}{2p}}B^{\mathrm{r}}_{\mathrm{qt},p}\delta^{\mathrm{r}}_{\mathrm{ecc.}}}{2\mu_0 L_{\mathrm{Qt},p+1}}\left(-1+\frac{1}{1-\mathrm{j}\omega^{\mathrm{r}}_{\mathrm{ecc.}}\left\{L_{\mathrm{Qt},p+1}/R_{\mathrm{Q},p+1}\right\}}\right)\mathrm{e}^{-\mathrm{j}\omega^{\mathrm{r}}_{\mathrm{ecc.}}}
\end{aligned}
\quad . \qquad (37)
$$

By substituting equations (37) into equation (33) the expression for the total electromagnetic force exerted on the eccentric rotor of a salient-pole synchronous machine can be rewritten

$$
\begin{aligned}
\underline{F}_{\mathrm{e}}^{\mathrm{r}} = \frac{\pi d_{\mathrm{r}} l_{\mathrm{e}}}{4\mu_0} \Bigg[& \left(\frac{{B_{\mathrm{dt},p}^{\mathrm{r}}}^{2}}{\delta_{0,\mathrm{d}}} + \frac{{B_{\mathrm{qt},p}^{\mathrm{r}}}^{2}}{\delta_{0,\mathrm{q}}} \mathrm{e}^{\mathrm{j}\frac{\pi}{2p}} \right) + \\
& + \frac{B_{\mathrm{dt},p}^{\mathrm{r}}}{2\delta_{0,\mathrm{d}}} \left(\frac{{k_{\mathrm{D},p-1}}^{2} L_{\mathrm{D},p-1} \left\{ B_{\mathrm{dt},p}^{\mathrm{r}} + \mathrm{j} B_{\mathrm{qt},p}^{\mathrm{r}} \right\}}{L_{\mathrm{Dt},p-1}} \left(-1 + \frac{1}{1 - \mathrm{j}\omega_{\mathrm{ecc.}}^{\mathrm{r}} \left\{ L_{\mathrm{Dt},p-1} / R_{\mathrm{D},p-1} \right\}} \right) + \right. \\
& \left. + \frac{{k_{\mathrm{D},p+1}}^{2} L_{\mathrm{D},p+1} \left\{ B_{\mathrm{dt},p}^{\mathrm{r}} - \mathrm{j} B_{\mathrm{qt},p}^{\mathrm{r}} \right\}}{L_{\mathrm{Dt},p+1}} \left(-1 + \frac{1}{1 - \mathrm{j}\omega_{\mathrm{ecc.}}^{\mathrm{r}} \left(L_{\mathrm{Dt},p+1} / R_{\mathrm{D},p+1} \right)} \right) \right) + \\
& + \frac{B_{\mathrm{qt},p}^{\mathrm{r}} \mathrm{e}^{\mathrm{j}\frac{\pi}{2p}}}{2\delta_{0,\mathrm{q}}} \left(\frac{{k_{\mathrm{Q},p-1}}^{2} L_{\mathrm{Q},p-1} \left\{ B_{\mathrm{qt},p}^{\mathrm{r}} - \mathrm{j} B_{\mathrm{dt},p}^{\mathrm{r}} \right\}}{L_{\mathrm{Qt},p-1}} \left(-1 + \frac{1}{1 - \mathrm{j}\omega_{\mathrm{ecc.}}^{\mathrm{r}} \left\{ L_{\mathrm{Qt},p-1} / R_{\mathrm{Q},p-1} \right\}} \right) + \right. \\
& \left. \left. + \frac{{k_{\mathrm{Q},p+1}}^{2} L_{\mathrm{Q},p+1} \left\{ B_{\mathrm{qt},p}^{\mathrm{r}} + \mathrm{j} B_{\mathrm{dt},p}^{\mathrm{r}} \right\}}{L_{\mathrm{Qt},p+1}} \left(-1 + \frac{1}{1 - \mathrm{j}\omega_{\mathrm{ecc.}}^{\mathrm{r}} \left\{ L_{\mathrm{Qt},p+1} / R_{\mathrm{Q},p+1} \right\}} \right) \right) \right] \delta_{\mathrm{ecc.}}^{\mathrm{r}} \mathrm{e}^{-\mathrm{j}\omega_{\mathrm{ecc.}}^{\mathrm{r}} t}
\end{aligned}
\quad . \quad (38)
$$

In this equation, electromagnetic force on the eccentric rotor of a salient-pole synchronous machine is represented as a function of whirling radius and whirling angular speed. Using complex- and real-valued parameters equation (38) can be rewritten as

$$
\frac{\underline{F}_{\mathrm{e}}^{\mathrm{r}}}{\delta_{\mathrm{ecc.}}^{\mathrm{r}} \mathrm{e}^{-\mathrm{j}\omega_{\mathrm{ecc.}}^{\mathrm{r}} t}} = K\left(\mathrm{j}\omega_{\mathrm{ecc.}}\right) = c_0 + \frac{c_{\mathrm{dm}}}{r_{\mathrm{dm}} - \mathrm{j}\omega_{\mathrm{ecc.}}^{\mathrm{r}}} + \frac{c_{\mathrm{dp}}}{r_{\mathrm{dp}} - \mathrm{j}\omega_{\mathrm{ecc.}}^{\mathrm{r}}} + \frac{c_{\mathrm{qm}}}{r_{\mathrm{qm}} - \mathrm{j}\omega_{\mathrm{ecc.}}^{\mathrm{r}}} + \frac{c_{\mathrm{qp}}}{r_{\mathrm{qp}} - \mathrm{j}\omega_{\mathrm{ecc.}}^{\mathrm{r}}} \ , \quad (39)
$$

here, $K\left(\mathrm{j}\omega_{\mathrm{ecc.}}\right)$ is the Frequency Response Function (FRF) of the electromagnetic force, c – are the complex-valued parameters and r – are the real-valued parameters.

Equation (39) is a low-order parametric model of the electromagnetic force on an eccentric rotor of a salient-pole synchronous machine. Model parameters can be estimated using the data obtained from impulse method applied in FEA. Thus, the model accounts for the effects of iron core saturation, slotting and equalising currents in the rotor cage because all these are considered in the FEA.

2.9 Brief description of impulse method

The impulse method is applied in the FEA by moving the rotor from its central position for a short period of time [14]. This displacement excitation disturbs the magnetic field by creating the permeance harmonics in the air gap and, by doing this, produces the force between the rotor and stator.

Displacement magnitude has to be large enough to enable the separation of eccentricity caused force from the noise or error of the finite element calculation. On

the other hand, in the region of excessively large eccentricity values the dependence of force magnitude on the eccentricity becomes non-linear. The questions related to linearity of the electromagnetic force are discussed in [16].

The results obtained from the impulse method are the electromagnetic force resolved into two orthogonal components and the position of the eccentric rotor at every sample of the simulation time. Thus, the FRF of the force can be readily calculated by dividing the cross-spectral density of the response (electromagnetic force) and excitation (rotor displacement) signals by the auto spectral density of the excitation signal [14].

Force model parameters can be estimated from the FRF of the force by combining the method of least squares and sequential exhaustive search.

As the impulse method was never before applied to the analysis of a synchronous machine the results obtained had to be verified using another approach. For this purpose numerous simulations were carried out using the conventional forced whirling method. In this method, the rotor was forced to move along a circular orbit at a constant velocity in the time-stepping FEA. More details on this method can be obtained from [13].

3 Results

To assess the performance of the force model developed, a salient-pole synchronous machine was simulated using the impulse method in FEA. The main parameters of the machine are listed in Table 1.

The machine was operated in a generator mode and connected to a constant line voltage. The mechanical angular velocity of the rotor was kept constant. The machine was equipped with rotor cage, the stator winding did not have parallel paths. The cross-section view of the machine is given on Figure 1.

Table 1. Main parameters of the simulated machine.

Parameter	Value
Number of pole-pairs	4
Frequency of the voltage supplied to the stator winding, Hz	50
Stator winding supply voltage, V	6300
Stator winding connection	Star
Field winding supply voltage, V	150
Apparent power, kVA	8356.6
Power factor	0.83 Cap.

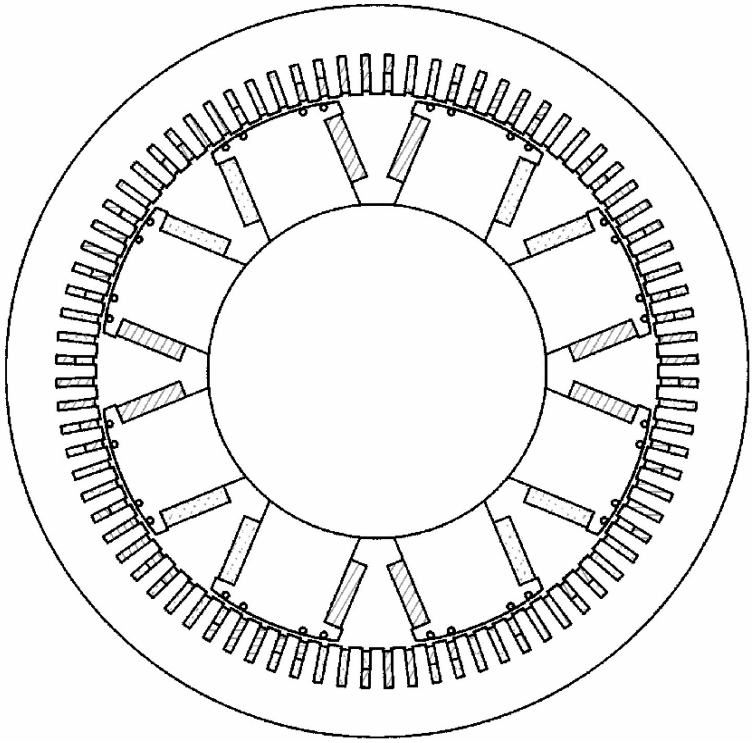

Figure 1. Cross-section view of the simulated machine.

The impulse excitation was introduced in FEA by displacing the rotor axis from the centred position for a short period of time. Rotor displacement had a shape $\varepsilon(t) = \varepsilon\left(1 - \cos\frac{2\pi t}{T}\right)$, $t_1 < t < t_2$. The amplitude of the excitation pulse ε was set to 10% of the air gap length. The period of the pulse was T = 0.01 s. The starting and ending time instants of the pulse were t_1 = 0.04 s and t_2 = 0.05 s. Two first seconds of the machine performance were simulated with a time step of 0.1 ms.

Using the results of impulse method the FRF of the force was calculated. This FRF is plotted on Figure 2. These results were also compared against the results from conventional forced whirling method.

Force model parameters estimated from the FRF of the force are listed in Table 2.

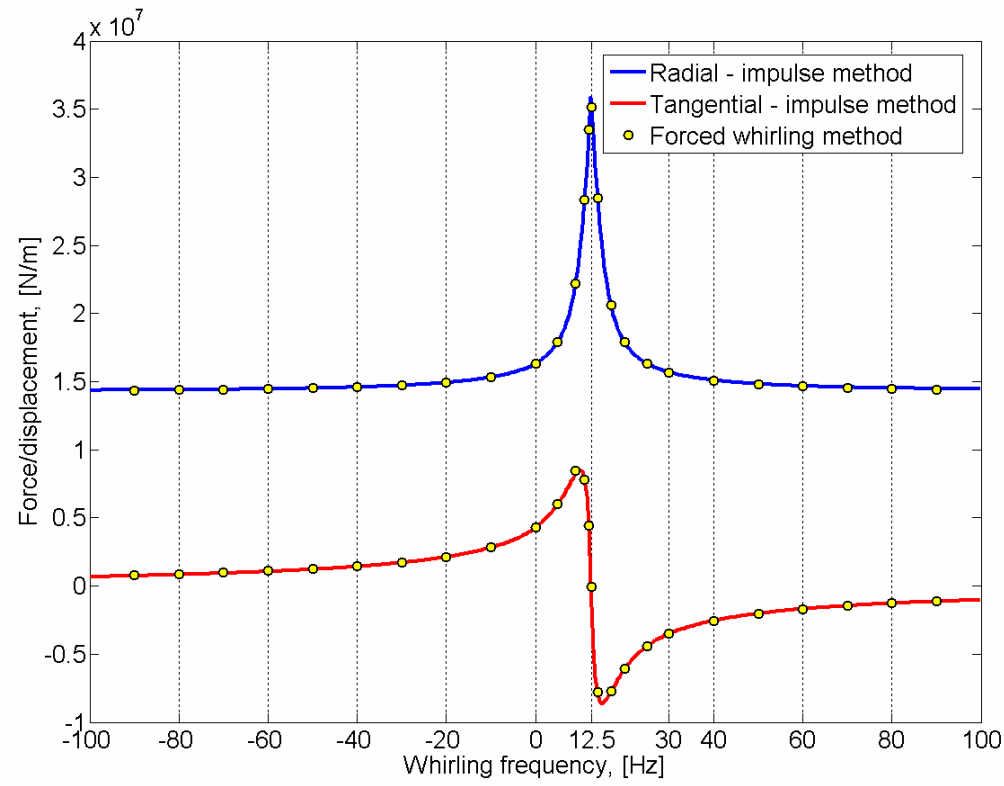

Figure 2. FRF of the force calculated using the impulse method results and comparison against the results from the forced whirling method.

Table 2. Estimated force model parameters.

Parameter	Value
c_0	1.43e+07 – j7.57e+04
c_{dm}	–1.85e+08 + j7.86e+05
c_{dp}	–2.01e+08 – j5.53e+06
c_{qm}	–1.45e+08 – j2.45e+05
c_{qp}	–5.07e+06 + j7.62e+03
r_{dm}	–30.41
r_{dp}	–176.69
r_{qm}	–12.50
r_{qp}	–1.89

To evaluate the accuracy of the presented force model these parameters were substituted into the force model expression (39). By doing this, the estimated FRF of the force was obtained. Comparison of the estimated FRF against the original FRF from the impulse method is shown on Figure 3.

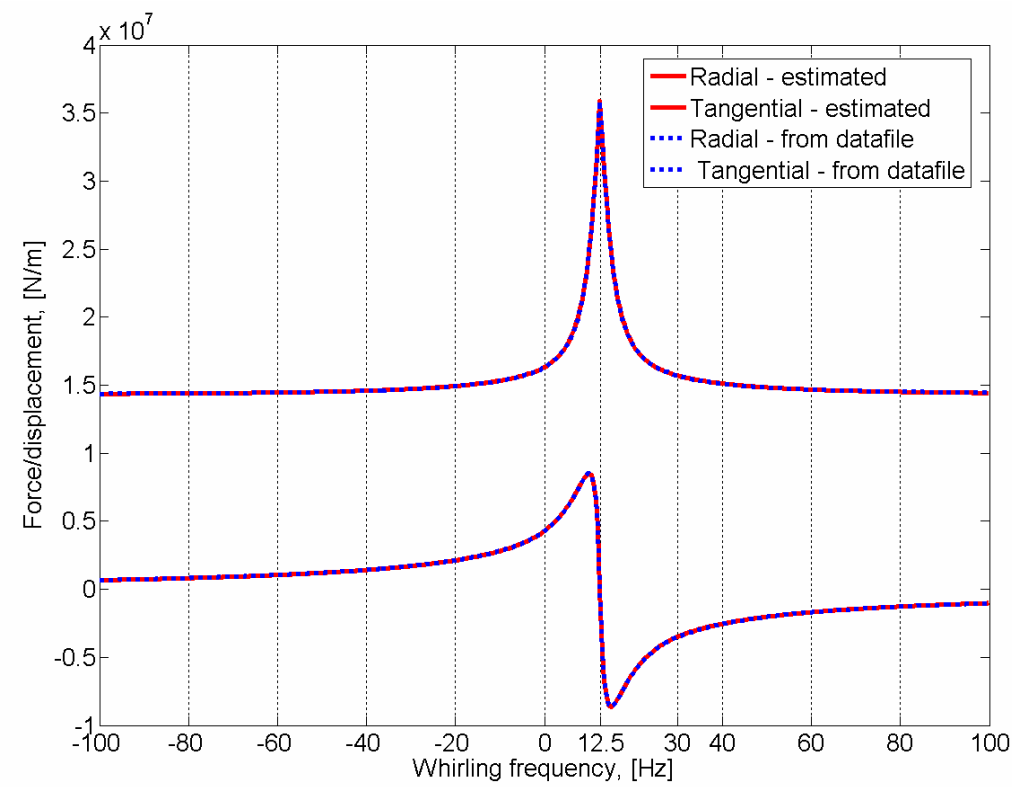

Figure 3. Comparing the FRF obtained using the parametric force model with estimated parameters against the FRF obtained from impulse method.

The error between absolute values of the two FRFs is presented on Figure 4.

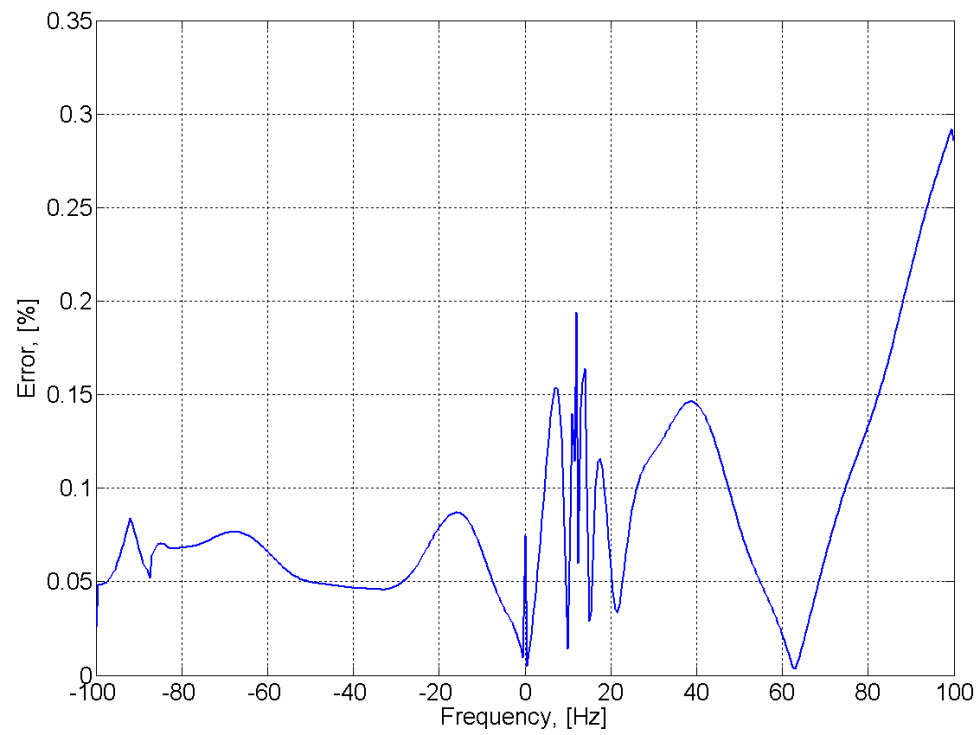

Figure 4. Error between the two FRF curves.

4 Discussions

The FRF of the force obtained from the impulse method (Figure 2) is resolved into two components: the radial one – acting in the direction of the shortest air gap length; and the tangential one, which is perpendicular to the radial one. The tangential component of the electromagnetic force due to the rotor eccentricity must be distinguished from the tangential force responsible for the machine's torque generation in normal operation. In this paper, the term "tangential component" will only refer to the electromagnetic force produced due to the rotor eccentricity.

As seen, the radial force component, being substantially stronger than the tangential component, provides the largest contribution to the net electromagnetic force.

According to Figure 2, the radial component of the electromagnetic force has a sharp peak at a whirling frequency of 12.5 Hz, which, for an eight-pole synchronous machine, is exactly the mechanical frequency of the rotor motion. This phenomenon is explained by the fact that at this particular whirling frequency value the $p \pm 1$ magnetic field harmonics due to the rotor eccentricity become stationary with respect to the damper winding and do not induce any voltage in it. As a result, $p \pm 1$ current harmonics in the damper winding vanish (see equations (37)). Thus, without being damped by the rotor currents the $p \pm 1$ components of the magnetic field are increased significantly causing the peak in the electromagnetic force curve at a whirling frequency of 12.5 Hz. Figure 2 also demonstrates that the damper winding very effectively attenuates the electromagnetic force due to the eccentric rotor, except at the whirling frequency of 12.5 Hz. It is also interesting to note that the tangential force component changes its sign at this whirling frequency value. In Figure 2, the results from impulse method are also verified by comparing them against the results from the conventional forced whirling method. A good agreement between the results demonstrates the suitability of the impulse method for the analysis of a synchronous machine. The main benefit of using the impulse method is the considerable saving of computational time. This method requires less than 5% of the computational time consumed by the conventional forced whirling method [14].

Figure 3 shows that the FRF obtained by substituting the estimated parameters into the force model expression closely follows the FRF provided by the impulse method. Figure 4 reveals that the maximal error between the absolute values of the two FRFs is about 0.3 %. The average error in the whirling frequency range from –100 to +100 Hz is less than 0.09 %, which is a fairly good result.

The presented force model has several advantages:

1) Simple, quick and accurate calculation of the electromagnetic force – By substituting the estimated parameters into the model expression the force at a certain whirling frequency value or in a certain range of whirling frequencies can be calculated in a matter of seconds.

2) Applicability at different whirling radius and whirling frequency values – When creating the force model it was assumed that the force is a linear function of the rotor displacement. Since the FRF represent the force per whirling radius in a certain range of whirling frequencies, the same model parameters can be used at different values of rotor eccentricity in that whirling frequency range. Again, there is no need to carry out the time-consuming finite element calculations.
3) An attractive opportunity to study the electromechanical interaction in electrical machines – The parametric force model integrated into the mechanical analysis of the machine would only marginally increase the computational burden of the calculations.

The presented force model has also several limitations. Firstly, the estimated set of force model parameters corresponds to a certain operating point of a machine. Once the operating point (supply voltage, load torque, etc.) is changed the FRF of the force must be recalculated and new parameters established. As it was said earlier the developed force model is valid for a synchronous machine, which is equipped with a rotor cage and has no parallel paths in the stator winding. The parallel paths in the stator winding having a very strong influence on the resultant magnetic field distribution in the air gap would considerably affect the shape of the FRF and, therefore, need a different force model to be applied. This is the topic for future research.

5 Conclusions

In this paper, the magnetic field in a salient-pole synchronous machine with eccentric rotor was studied. Based on the theory elaborated and results acquired a low-order parametric force model for the machine has been developed and verified. Force model parameters were calculated from the results provided by the impulse method applied in the FEA. The force model with estimated parameters showed an excellent performance in a wide whirling frequency range.

The proposed force model has the following advantages:

1) It allows simple, quick and accurate calculation of the electromagnetic force at a desired whirling frequency value or in a certain range of whirling frequencies
2) The same model parameters can be directly used at different values of whirling radius and whirling frequency
3) The model offers an attractive opportunity to be integrated into the mechanical analysis to study the electromechanical interaction in electrical machines.

The limitations of the force model are:

1) Every time the operating point (supply voltage, load torque, etc.) of a machine is changed the FRF of the force has to be recalculated and a new set of force model parameters established
2) The model is not applicable for a synchronous machine with parallel paths in the stator winding.

Besides, results presented in this paper have also verified the suitability of the computationally efficient impulse method for the analysis of a synchronous machine.

References

[1] J. Fisher-Hinnen (1899) "Dynamo design", Van Nostrand.

[2] A. C. Smith, D. G. Dorrell "Calculation and measurement of unbalanced magnetic pull in cage induction motors with eccentric rotors. Part 1: Analytical model", *IEE Proceedings: Electric Power Applications*, vol. 143, No. 3, May, 1996, pp. 193 - 201.

[3] R. Belmans, A. Vandenput and W. Geysen, "Influence of unbalanced magnetic pull on the radial stability of flexible-shaft induction machine", *IEE Proceedings, Electric Power Applications*, Vol. 134, No.2, Part B, March 1987, pp. 101 - 109.

[4] A. Stavrou, J. Penman, "Modelling dynamic eccentricity in smooth air-gap induction machines", *Electric Machines and Drives Conference, IEMDC 2001*, *IEEE International*, 2001, pp. 864 - 871.

[5] S. Fruchtenicht, E. Pittius, H. O. Seinsch, "A diagnosting system for three-phase asynchronous machines", *Electric Machines and Drives, Fourth International Conference*, Conf. Publ. No. 148, September 13-15, 1989, pp. 163 - 171.

[6] G. M. Joksimovic, M. D. Durovic, J. Penman, N. Arthur, "Dynamic Simulation of Dynamic Eccentricity in Induction Machines – Winding Function Approach", *IEEE Transactions on Energy Conversion,* Vol. 15, No. 2, June 2000, pp.143 – 148.

[7] N. A. Al-Nuaim, H. A. Toliyat, "A method for dynamic simulation and detection of dynamic air-gap eccentricity in synchronous machines", *Proceedings of the IEEE International Electric Machines and Drives Conference*, May 18-21 1997, Milwaukee, USA, pp MA2 5.1 - 5.3.

[8] H. A. Toliyat, N. A. Al-Nuaim, ”Simulation and detection of dynamic air-gap eccentricity in salient pole synchronous machine”, *IEEE Industry Applications Society Annual Meeting*, October 5-9 1997, New Orleans, USA, pp. 255 - 262.

[9] N. A. Al-Nuaim, H. A. Toliyat, “Novel method for modeling dynamic air-gap eccentricity in synchronous machines based on modified winding function theory”, *IEEE Transactions on Energy Conversion*, vol. 13, No. 2, June 1998, pp. 156 – 162.

[10] A. Arkkio, O. Lindgren, “Unbalanced magnetic pull in a high-speed induction motor with an eccentric rotor”, *Proceedings of the International Conference on Electrical Machines*, 5-8 September 1994, Paris, France, Vol. 1, pp. 53 – 58.

[11] D. G. Dorrell, “Calculation of unbalanced magnetic pull in small cage induction motors with skewed rotors and dynamic rotor eccentricity”, *IEEE Transactions on Energy Conversion*, Vol. 11, No. 3, September 1996, pp. 483 – 488.

[12] J. Früchtenicht, H. Jordan and H. O. Seinsch, “Exzentrizitätsfelder als Ursache von Lafinstabilitäten bei Asynchronmaschinen. Teil I und II”, *Archiv fur Elektrotechnik*, Vol. 65, 1982, pp. 271 – 292.

[13] A. Arkkio, M. Antila, K. Pokki, A. Simon and E. Lantto, “Electromagnetic force on a whirling cage rotor”, *IEE Proceedings, Electrical Power Applications*, vol.147, September 2000, pp. 353 – 360.

[14] A. Tenhunen, T. P. Holopainen and A. Arkkio, “Impulse Method to Calculate the Frequency Response of the Electromagnetic Forces on Whirling Cage Rotors”, *IEE Proceedings, Electrical Power Application*, Vol. 150, No. 6, 2003, pp. 752-756.

[15] Taegen F (1964) Die Bedeutung der Läufernutschlitze für die Theorie der Asynchronmaschine mit Käfigläufer. Arch. für Electrotechnik 48: 373-386.

[16] A. Tenhunen, T. P. Holopainen, A. Arkkio, “Spatial linearity of unbalanced magnetic pull in induction motors during eccentric rotor motions”, *COMPEL: The International Journal for Computation and Mathematics in Electrical and Electronic Engineering*, Vol. 22, No. 4, 2003, pp. 862 – 876.